REPORT DOCUMENTATION PAGE

Form Approved
OMB No. 0704-0188

PLEASE DO NOT RETURN YOUR FORM TO THE ABOVE ORGANIZATION.

1. REPORT DATE *(DD-MM-YYYY)*	2. REPORT TYPE	3. DATES COVERED *(From - To)*
06-06-2009	Final Report	1 Mar 06 - 30 Nov 09

4. TITLE AND SUBTITLE

Preparation of Oxidation-Resistant Ultra High Melting Temperature Materials and Structures Using Laser Method

5a. CONTRACT NUMBER

5b. GRANT NUMBER

FA9550-06-1-0163

5c. PROGRAM ELEMENT NUMBER

6. AUTHOR(S)

Gupta, Mool C.

5d. PROJECT NUMBER

5e. TASK NUMBER

5f. WORK UNIT NUMBER

7. PERFORMING ORGANIZATION NAME(S) AND ADDRESS(ES)

Department of Electrical and Computer Engineering
University of Virginia
351 McCormick Road, P.O. Box 400743, Charlottesville, VA 22904

8. PERFORMING ORGANIZATION REPORT NUMBER

9. SPONSORING/MONITORING AGENCY NAME(S) AND ADDRESS(ES)

AFOSR
875 N. Randolph St.
Suite 325
Arlington, VA 22203

10. SPONSOR/MONITOR'S ACRONYM(S)

AFOSR

11. SPONSOR/MONITOR'S REPORT NUMBER(S)

AFRL-OSR-VA-TR-2012-0404

12. DISTRIBUTION/AVAILABILITY STATEMENT

A

13. SUPPLEMENTARY NOTES

14. ABSTRACT

This report describes laser and hybrid (laser + microwave) processing of ultra-high temperature ceramic (UHTC) materials. We have successfully developed new UHTC based composite materials that are capable of dealing with harsh environment encountered by hypersonic cruise and atmospheric re-entry vehicles. The advanced ZrB2-metal composites provide good performance at much lower densities than other UHTCs like hafnium diboride (HfB2) and refractory metals such as rhenium and tungsten. In addition, these ceramic-metal composites (cermets) reduce the likelihood of mechanical failures by increasing fracture toughness and thermal shock resistance that are inherent properties of mostly brittle ceramics, but at the same time enhance some material properties like hardness that usually lack in metals.

15. SUBJECT TERMS

16. SECURITY CLASSIFICATION OF:			17. LIMITATION OF ABSTRACT	18. NUMBER OF PAGES	19a. NAME OF RESPONSIBLE PERSON
a. REPORT	b. ABSTRACT	c. THIS PAGE		36	Prof. Mool C. Gupta
					19b. TELEPHONE NUMBER *(Include area code)* 757-325-6850

Reset

Standard Form 298 (Rev. 8/98)
Prescribed by ANSI Std. Z39.18

FINAL REPORT

Preparation of Oxidation-Resistant Ultra High Melting Temperature Materials and Structures Using Laser Method

Principal Investigator:
Professor Mool C. Gupta
Department of Electrical and Computer Engineering
University of Virginia
351 McCormick Road, P.O. Box 400743
Charlottesville, Virginia 22904-4743
Phone: 757-325-6850
Fax: 757-325-6988
e-mail: mgupta@virginia.edu

Participants:
Chen-Nan Sun and Tyson Baldridge

Contract: AFOSR Award # FA9550-06-1-0163
Program Manager: Dr. Joan Fuller

Date: June 2009

EXECUTIVE SUMMARY

This report describes laser and hybrid (laser + microwave) processing of ultra-high temperature ceramic (UHTC) materials. We have successfully developed new UHTC based composite materials that are capable of dealing with harsh environment encountered by hypersonic cruise and atmospheric re-entry vehicles. The advanced ZrB_2-metal composites provide good performance at much lower densities than other UHTCs like hafnium diboride (HfB_2) and refractory metals such as rhenium and tungsten. In addition, these ceramic-metal composites (cermets) reduce the likelihood of mechanical failures by increasing fracture toughness and thermal shock resistance that are inherent properties of mostly brittle ceramics, but at the same time enhance some material properties like hardness that usually lack in metals.

General methods to densify UHTCs include hot pressing and spark plasma sintering, but most methods are limited to producing simple-shaped objects. To address this issue, we have attempted using radiation sources like laser, microwave, electron beam (e-beam) and hybrid sintering techniques to build structures layer by layer from powders. Thus, fabrication of complex 3-dimensional (3-D) objects is feasible. However, energy sources like laser and e-beam need to focus on a small area during sintering while scanning the beam to achieve the desired final structure. Scanning creates a high temperature gradient between the beam center and the surroundings that generates thermal stress which can prevent proper structure formation. Processing UHTCs accentuates the problem due to the high delta-T involved. To alleviate this problem, high melting point materials having adequate ductility and fracture toughness are mixed into UHTC powders as a binding interface between particles. Results on ZrB_2-metal composites have shown that cracks usually seen on pure ZrB_2 sintered layers can be substantially suppressed. Although a few voids still exist in the sintered objects, the overall density is still greater than 98% of maximum. Moreover, ZrB_2-metal composites have great performance in Vickers microhardness tests that is analogous to the value of bulk ZrB_2. Furthermore, very high power lasers (kW range) and hybrid sintering using microwave or induction heating as additional energy sources can provide a uniform thermal profile that complements the laser sintering process. Using multiple modes of heating can decrease the processing time and allow for thicker samples to be processed per treatment. On the other hand, microwave processing also allows for unique nano-structure growth on the surface of treated samples, which could then be used to facilitate bonding multiple layers or in other novel applications.

The approaches and progress discussed in this report are stepping stones for further exploration of these novel UHTC-metal composites that can benefit various applications in aerospace, nuclear and high temperature electronics industries. The knowledge learned here can contribute to the designing of more reliable materials under severe thermal stress or shock to avoid mechanical failures. Thus, creating functional cermets from composition modification needs more studies for applicability, oxidation resistance and thermal fatigue behaviors.

OUTLINE

I. INTRODUCTION

Ultra-high temperature ceramics (UHTC) are a group of materials having high strength and high oxidation resistance that are suitable for certain applications in aeronautics and space industry. In the past few years, zirconium diboride (ZrB_2) and its composites have gained more attention because they provide similar performance at much lower densities compared to other widely studied UHTC materials like hafnium diboride (HfB_2) and current nozzle materials such as rhenium and tungsten.

Research on densification of UHTCs including hot pressing, pressureless sintering, and spark plasma sintering has been reported [1, 2]. Although hot pressing is an effective technique for densification, it is limited to producing simple shapes. To solve this problem, we have attempted using radiation sources such as laser, electron beam and microwave in this study.

Laser sintering is a rapid prototyping technique that builds objects layer by layer from powders. When the laser beam irradiates the powder surface, the powder absorbs light energy and the temperature rises, causing necking, grain growth, partial or full melting, and eventually densification. Moreover, it is a non-contact process, so contamination is minimized. However, due to the relatively small beam size, this technique requires a beam or sample scanning to cover a large area.

Electron beam sintering is also a layer additive process that can build complex 3-dimentional structures directly via computer controlled technique. When the electron beam is directed to the powder surface, the kinetic energy is instantly converted into thermal energy. The surface temperature around the beam rises substantially and powder materials begin to consolidate. The high energy electron beam can fully melt the particles to produce a void-free part. Electron beam sintering technique is primarily limited to conductive materials like metals and their alloys so that the electron charge can be dissipated. Most ceramics are electrically non-conductive; however, ZrB_2 has significant electrical conductivity hence it was considered for electron beam sintering.

Microwave heating works well for large volumes, but ceramics normally have a low dielectric absorption constant at room temperatures for microwave frequencies. A susceptor is typically used to facilitate the initial absorption. For an electrically conductive material like ZrB_2, however, arc heating can also stimulate absorption. Furthermore, the arcing can create a local plasma hot enough to sinter UHTCs.

This project investigated laser, microwave, electron beam and hybrid sintering of ZrB_2 powders and cermets. The report describes the experimental details and results obtained for various sintering conditions.

II. EXPERIMENTAL

Schematic of experimental setups of hybrid sintering systems.

(a) High power CW laser sintering system with induction heating capability

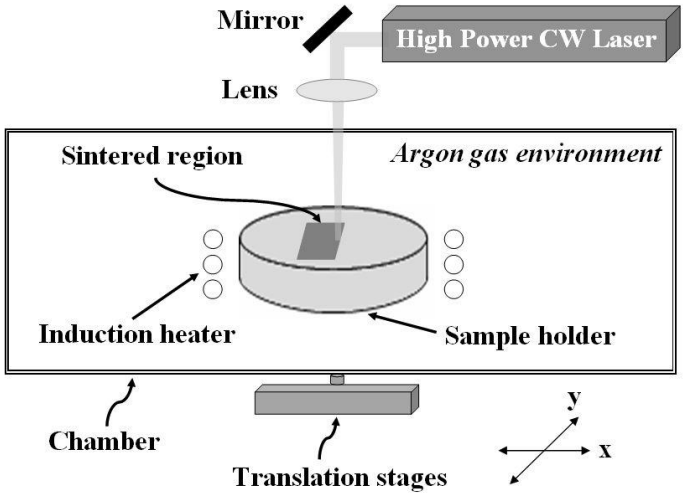

(b) Microwave + laser sintering system

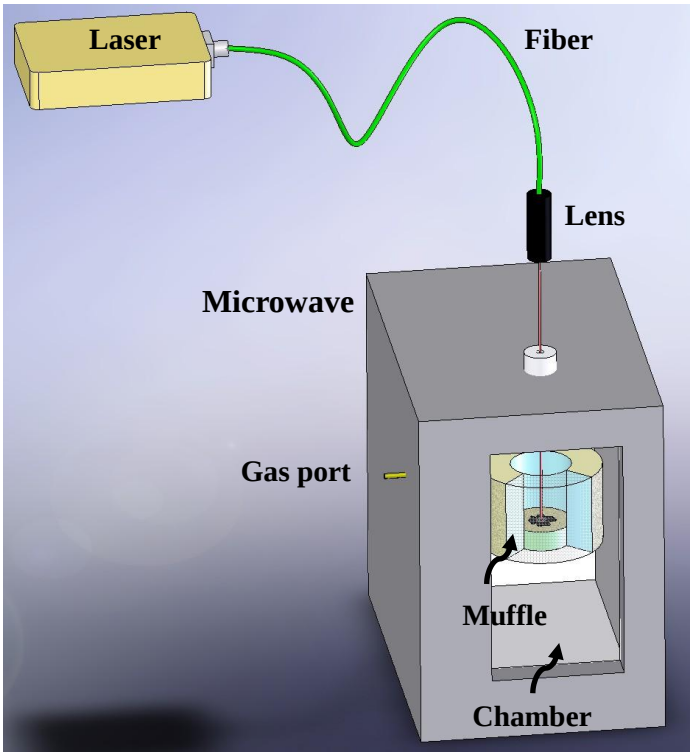

A. Laser sintering system:

High power continuous wave (CW) laser with wavelength of 940 nm is used. Applied laser power is between 65 and 152 W, with beam spot size from 0.5 to 4 mm. Other process parameters included scan line overlapping between 60% and 80%, scan speed ranging from 0.6 to 4 mm/s. In addition, an RF induction heater can provide substrate and sample preheating and/or additional heating during the sintering process. Specifications for the laser, induction heater, and translation stages and motion controller are the following:

- CW fiber-coupled diode laser:
  a. Jenoptik JOLD-300-CPXF-2P2.
  b. ~250 W maximum output power (@140 A).
  c. Wavelength: 940 nm.
  d. SMA port through 2 m long, 400 µm fiber.
  e. 1:2 objective gives minimum 800 µm spot size at 110 mm.

- High-frequency alternating current (AC) induction heater:
  a. MTI corporation SP-15A desk-top induction heater.
  b. ~7 kW maximum output power.
  c. 20-100 kHz output frequency.

- Translation stages and motion controller:
  a. Newmark Systems Inc. NLS4/NSC-M.
  b. Resolution: 0.03 µm @ 50000 steps/rev motor resolution.
  c. Maximum travel speed: 12 mm/s.
  d. Maximum load: 50 lbs.

B. Microwave + laser sintering system:

The same Jenoptik CW laser is used but the sample is located within a microwave. Applied laser power is varied from 135 to 166 watts, with a stationary spot size ranging from 3 to 8 mm. Microwaves simultaneously radiate the sample within a small ceramic muffle. The microwave absorption coefficient of most ceramics is low, but increases with temperature. Thus, as the laser raises the temperature of the sample, microwave absorption in the sample increases in a positive feedback mechanism. This absorption can be increased using additives with higher absorption

coefficients. Silicon carbide has a higher loss tangent at 2.4 GHz than most ceramics, and thus absorbs microwave radiation more efficiently than ZrB_2 and the enclosing ceramics. SiC can be used to indirectly heat the sample via thermal radiation, or it can be mixed directly with the powder. SiC is commonly mixed with ZrB_2 even in standard sintering methods as it has a melting point approaching that of UHTCs (~3000 K) and it can improve the oxidation resistance of ZrB_2 to at least 1600 °C [3].

Specifications for the microwave and muffle are the following:

Muffle 1

- Microwave:
  a. Microwave Research & Applications, Inc. BP-1700.
  b. 1415 watts maximum output power.
  c. 2.4 GHz output frequency / 12.5cm wavelength.
  d. Cavity dimensions: 13” W x 12” D x 6.9” T.

- Muffle 1:
  a. Very-low-density alumina/silica sheets (white).
  b. 1" wall thickness
  c. Sheets glued with ceramic epoxy.
  d. Inside dimensions: 3” W x 3” D x 6” T.
  e. 2 separate penetrations for argon & laser, plus removable door

- Muffle 2:
  a. Medium-density alumina silicate (gray).
  b. 0.25" wall thickness.
  c. 2 halves with clamshell fit.
  d. Inside dimensions: 2.5” W x 2.5” D x 3.6” T.
  e. 1 common penetration for laser + argon, plus seam for clamshell.
  f. Sample resting on Si_3N_4 plate, on top of Al_2O_3 crucible.

C. Materials:

- UHTC: ZrB_2 powder has particle size distribution ranging from 0.5 to 6 μm with an average size of around 2 μm (Grade B, H.C. Starck, Germany). The provided composition by weight percent was: >18.5% B, <0.2% C, <1.5% O, <0.25% N, <0.1% Fe, >0.2% Hf, with the remainder zirconium. In some cases when heating via microwave, a ZrB_2 powder of -325 mesh was used (ZR-201, Micron Metals, Inc). Thus, all particles were < 44 micron with an average

near 15 μm. The provided composition by weight percent was: 76.4% Zr, 18.1% B, and 0.81% C, with typical impurities of <1.6% B_2O_3, <1% O_2, <0.2% N_2, and <0.2% Fe.

- Binding materials: Zr, Ti, Ta and Si are from Alfa Aesar, USA. Ni is from Atlantic Equipment Engineers, USA. Some material properties are listed in Table 1.

- ZrB_2-metal composites: Materials are weighed using an electronic balance (accuracy of 0.0001g) and then ball-milled for 24 hours. Table 2 shows weight percent of binder materials, with the remainder being ZrB_2.

Table 1. Properties of binding materials

Material	Melting point (°C)	Density (g/cm^3)	Purity (%)	Particle size (μm)	Product #
Zr	1857	6.49	> 98	2-3	00847
Ti	1668	4.51	> 99.5	< 44	42624
Ta	2996	16.65	> 99.6	< 44	10345
Si	1410	2.33	99.999	1-5	44185
Ni	1453	8.91	99.9	1-5	NI-101
Al_2O_3	2072	3.97	99.99	1-2	AL-601

Table 2. Compositions of powder mixtures used*

Binder material	Weight percent (wt%)			
Zr	40	35	30	20
Ti	50	35	30	20
Ta	50	35	30	20
Si	50	35	30	20
Ni	50	—	—	—

* The remainder is ZrB_2.

D. Sample holder and preparation:

Graphite sheet (McMaster-Carr, USA) is cut into different sizes and shapes to hold the powder materials. The graphite sample holders are 3/8" thick, with a width and length greater than ½" x ½" but less than 2" x 2". A section of graphite from the top surface is then removed to act as a container for the powder. Before sintering, the powder is pressed by hand using a metal die to decrease porosity as much as possible.

III. RESULTS AND DISCUSSION

A. Laser Processing:

i. Laser parameters:

A series of experiments were performed to determine suitable laser sintering/melting parameters for ZrB_2. Figure 1 shows effects of laser energy densities and the corresponding surface morphologies of sintered ZrB_2 objects. In Fig 1(a) and (b), necking has begun and tiny particles (< 1 μm) have all fused to larger ones (~ 2 μm). When the laser energy density was increased to 1.3 kJ/cm^2, even larger particles are fused together as shown in Fig 1(c), although voids are still common in the sintered layer. Finally, at 2.5 kJ/cm^2 and above, the temperature of the laser-processed region is high enough to melt and voids are filled. Fig 1(d) and (e) show the fully melted layer and the substantial grain growth.

Studies on the laser energy density dependence of binding materials were also performed. With beam spot size kept at ~ 2 mm, 90 W of laser power can start to melt silicon, titanium and zirconium powders. The melted region is very localized and the sintered regions still contain significant voids. Therefore, higher power of 130 - 150 W is needed for full melting of Si, Ti and Zr. However, tantalum and pure ZrB_2 have significantly higher melting points and are difficult to melt at these laser parameters

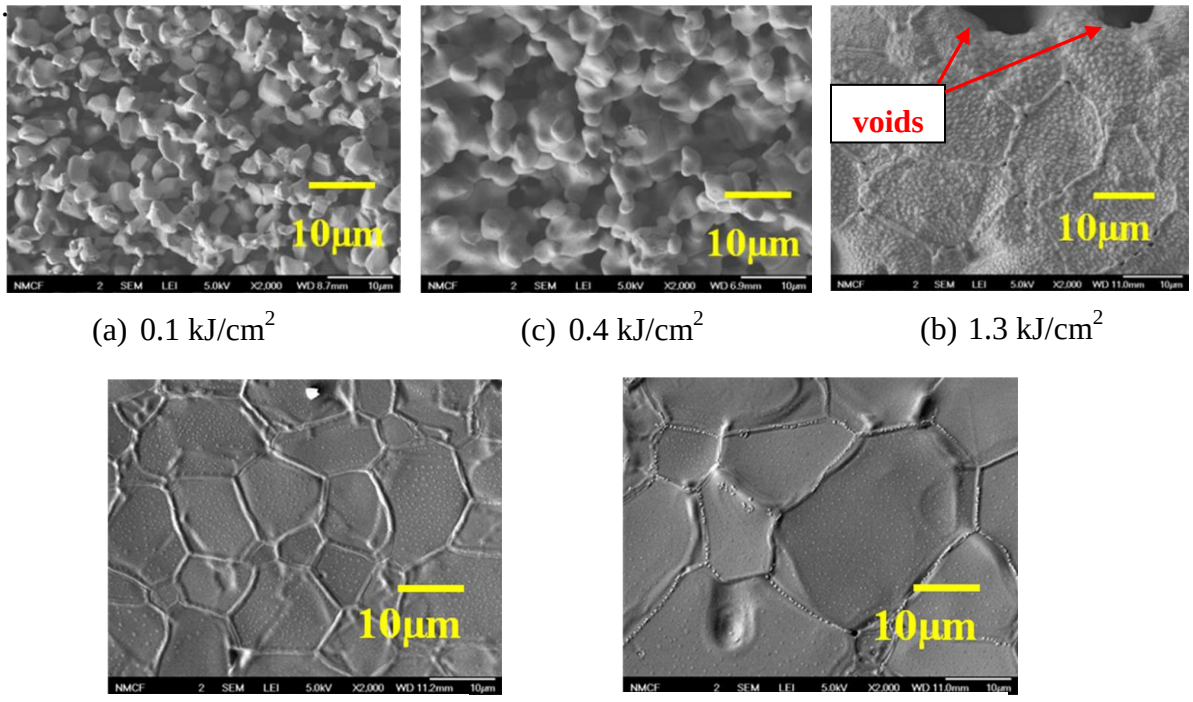

(a) 0.1 kJ/cm^2 (c) 0.4 kJ/cm^2 (b) 1.3 kJ/cm^2

(e) 2.5 kJ/cm^2 (d) 3.9 kJ/cm^2

Figure 1. Effects of laser energy densities on surface morphologies of sintered ZrB_2 objects.

ii. Effects of scanning patterns:

Three main scanning patterns (shown in Figure 2) have been used for thermal stress studies. These patterns are sometimes mixed during sintering experiments for stress relief.

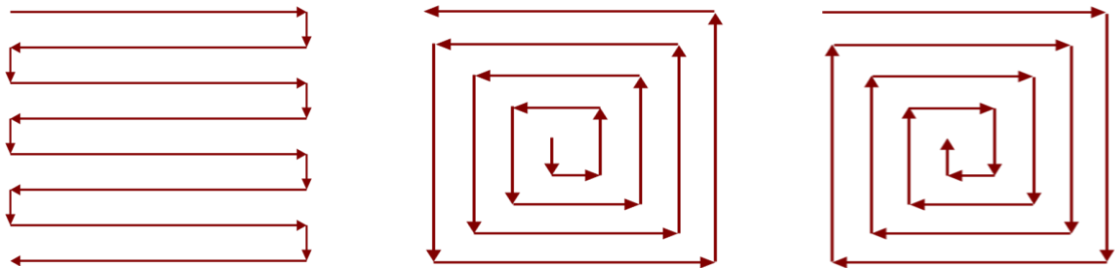

Figure 2. (a) (b) (c)

Scanning patterns: (a) serpentine (b) outward spiral from center and (c) inward spiral toward center.

Sintered results following patterns given in Figure 2 are shown in Figure 3 accordingly. For serpentine scanning pattern (Fig 3(a)), gaps are easily found along the scanning line because of the volume shrinkage arising from densification and the thermal stress caused by temperature gradients. In case of outward and inward spiral patterns shown in Fig 3(b) and (c), gaps formed in a different manner. The object's center is very well bound, but gaps occur along the outskirts. This can be explained as the shrinking rates of the structure are different between the center and the outskirt region. Likewise, the structural deformation is also not the same as in the serpentine pattern. Since spiral patterns produce better results, we have adopted them as our standard patterns. Nonetheless, in order to further reduce the thermal stress and gaps caused by volume shrinkage, more complex scanning patterns and/or an additional heating could improve results. Note that all powder mixtures result in similar structure shrinkage forms at each respective scanning pattern, although we only show three typical ones in Fig 3.

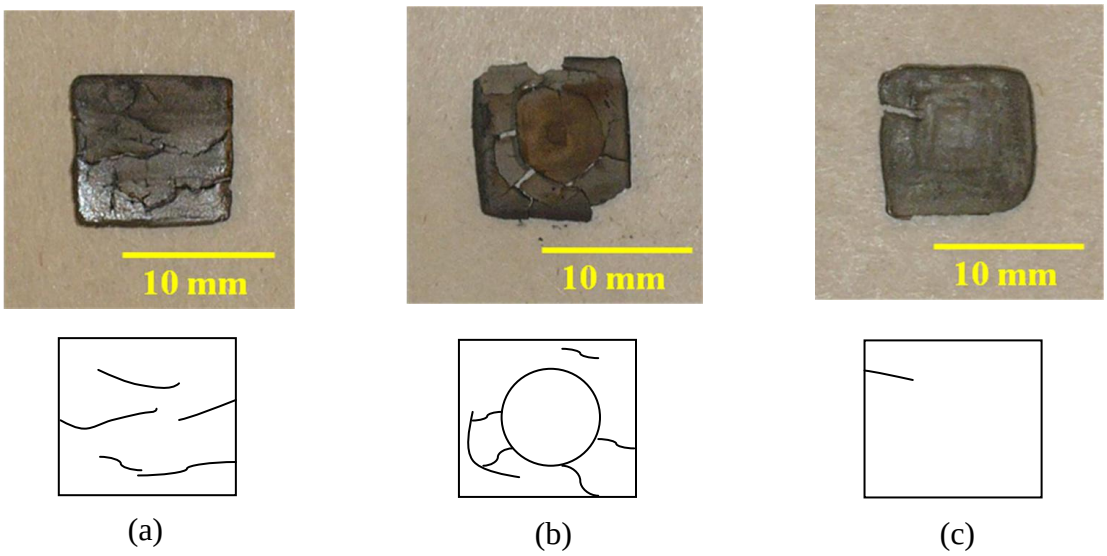

Figure 3. Sintered objects using different scanning patterns: (a) serpentine (50wt% Si + 50wt% ZrB_2); (b) outward spiral from center (50wt% Ta + 50wt% ZrB_2); (c) inward spiral towards center (50wt% Ti + 50wt% ZrB_2). Bottom three schematics are locations of major gaps for each sample respectively.

iii. Induction heating:

Thermal stress arises from temperature gradients between the laser beam irradiating region on the sample and its surroundings. It can induce structural deformation or even break the integrity of the samples. In order to mitigate the thermal stress, an induction heater is used to provide homogenous preheating during the laser sintering/melting process. The induction heater consists of a high-frequency alternating current passing through a copper coil which surrounds the sample. Any electrically conducting object inside the coil generates eddy currents to oppose the change of the magnetic field and subsequently causes joule heating. It should be noted that the sample holder (graphite), ZrB_2 and binding materials (Zr/Ti/Ta/Ni) are all conductive materials and therefore respond to inductive heating.

iv. Multi-layer structures:

Laser sintering is a rapid prototyping technique that builds near net shape 3-D structures layer by layer from powder materials. Layer thickness differs from sample to sample, depending on material compositions, laser parameters and substrate preheating. In general, layer thickness between 100 and 500 μm has been used in our studies. Figure 4 shows several multilayer objects fabricated in our lab. Note that Figure 4(a)-(c) are samples without post processing or surface finishing, but Figure 4(d) is a polished one.

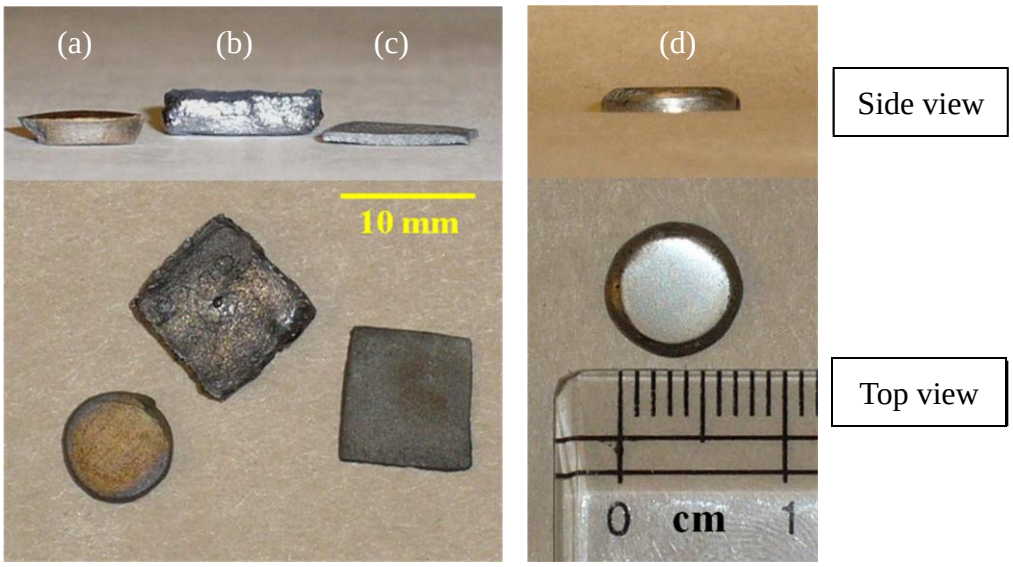

Figure 4. Sintered objects (a) 40wt% Zr + 60wt% ZrB_2 (b) 50wt% Si + 50wt% ZrB_2 (c) 30wt% Si + 70wt% ZrB_2 (d) polished 40wt% Zr + 60wt% ZrB_2 sample.

v. Microstructure & Composition:

Microstructures are discussed in terms of different powder mixtures in the following order: Zr-ZrB_2, Ti- ZrB_2, Ta- ZrB_2 and Si- ZrB_2.

1. Zr-ZrB_2 composite

Comparison of mixture compositions

Sintered objects are generally highly-densified and smooth throughout the entire sample. As shown in Figure 5(a), Zr and ZrB_2 are very well mixed and bound together. It is very difficult to know the composition of individual grain by simply looking at the SEM image. In the case of lower Zr concentration as shown in Figure 5(b), the morphology is different and ZrB_2 grains are now surrounded by Zr. It might be caused by the capillary action of molten Zr along ZrB_2 particles during sample processing. Their compositions have also been confirmed by energy-dispersive X-ray spectroscopy (EDS).

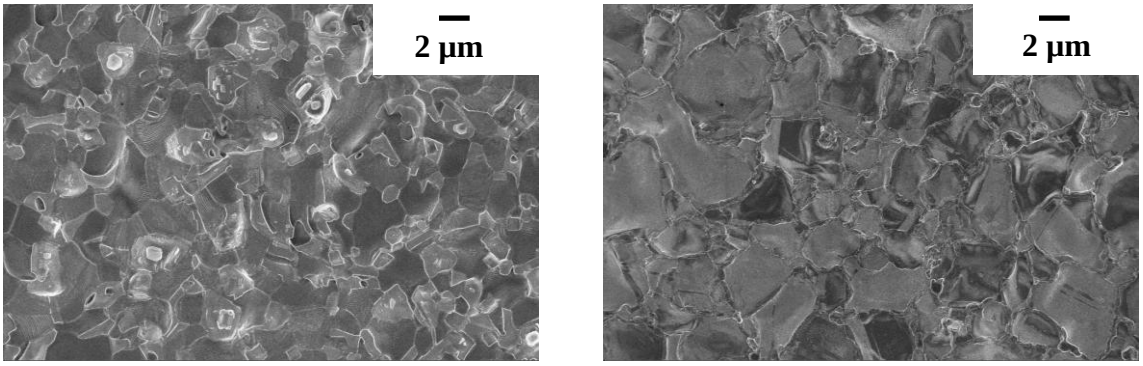

(a) (b)

Figure 5. SEM images (top view) of sintered objects: (a) 40wt% Zr + 60wt% ZrB_2 (b) 30wt% Zr + 70wt% ZrB_2.

Effect of laser parameters

The effect of laser power is shown in Figure 6. Voids are easily seen when the power used is only 130 W (Fig 6(a) points out some of these voids), but only a tiny one can be found at 150 W. This is easy to understand because higher power means the laser can provide more heat and therefore facilitate sintering or melting if other parameters stay the same.

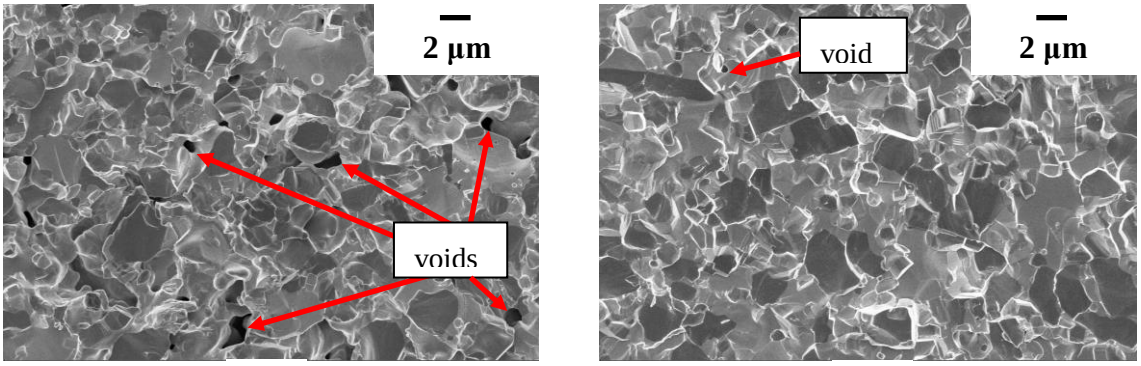

(a) (b)

Figure 6. SEM images (side view) of sintered objects: (a) laser power at 130 W (b) 150 W. Powder mixture is 40wt% Zr + 60wt% ZrB_2. Other process parameters include 2 mm spot size and 0.6 mm/s scanning speed.

Densification profile

Figure 7(a) shows the fully-densified top surface of a layer. However, voids begin to appear when we look deeper into the layer as shown in Figure 7(b). That means temperature gradients exist during laser sintering/melting process because the sample surface absorbs more of the laser energy. Results can be improved in two ways: (1) use a thinner powder layer for sintering or (2) use induction preheating.

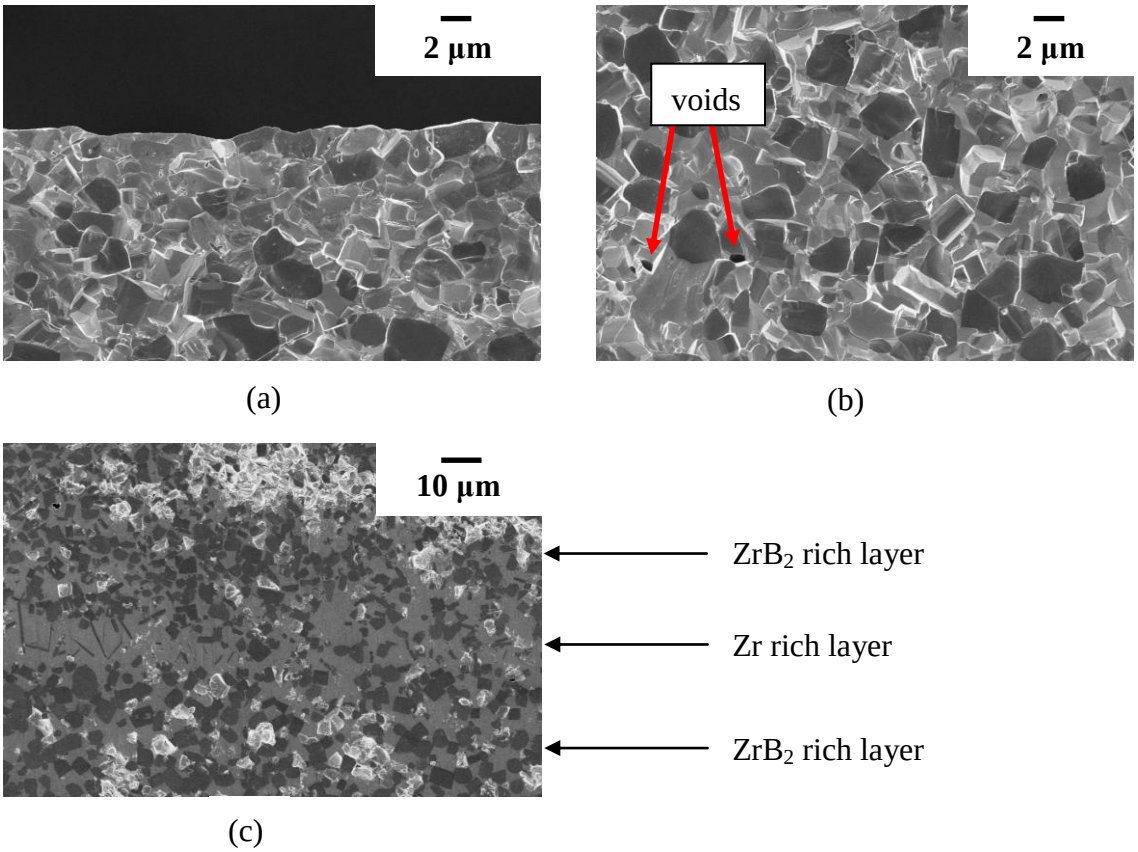

Figure 7. SEM images (side view) of sintered objects: (a) upper part (b) ~200 µm below top surface (c) layer interface of the polished sample. Powder mixture is 30wt% Zr + 70wt% ZrB_2.

Layer interface

Microstructures at the layer interface are especially important because good joints between layers are the major challenge for achieving a successful laser sintering/melting process. Figure 7(c) shows a layer of Zr-rich phase formed due to the Zr diffusion towards the interface between two layers of the ZrB_2-rich phase. In some cases the Zr-rich phase is more vague and difficult to distinguish it from the ZrB_2-Zr layer. Moreover, the Zr-rich phase may become weak points under mechanical or thermal stress and cause the structural failure. Therefore, a homogeneous sintered object is still more desired and may be realized through a more precise controlled process.

2. Ti-ZrB_2 composite

Some ZrB_2-metal composites can form new boride phases during laser processing, especially when binder materials possess similar chemical properties to Zr. We have observed the formation of new boride phases when Ti and Ta binder materials are used. Figure 8 shows TiB fibers spread around sintered sample. It is clear that as the Ti concentration increases so does the

yield of fibers. Moreover, fibers can act as reinforcement to the existing materials. It is known that fiber-reinforced materials can increase the strength and resistance to deformation. More research on Zr-TiB-ZrB_2 composites would allow further understanding the impact of fiber growth.

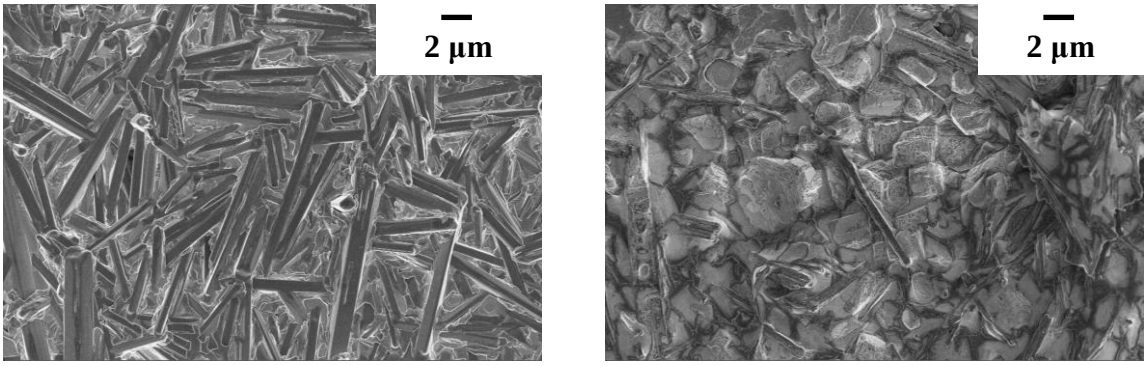

(a) (b)

Figure 8. SEM images (top view) of sintered: (a) 50wt% Ti + 50wt% ZrB_2 (b) 30wt% Ti + 70wt% ZrB_2.

3. Ta-ZrB_2 composite

Unlike other binder materials used in our studies, the melting point of Ta is near 3000°C, so it is very difficult to melt Ta under current laser parameters. Figure 9 shows voids are still widespread on the sintered sample, since the large grit Ta powder has not fully melted. This is different from ZrB_2-Ti mixture, where molten Ti has homogeneously spread and wetted surrounding ZrB_2 grains. Note both Ta and Ti have particle size of -325 mesh (< 44 µm).

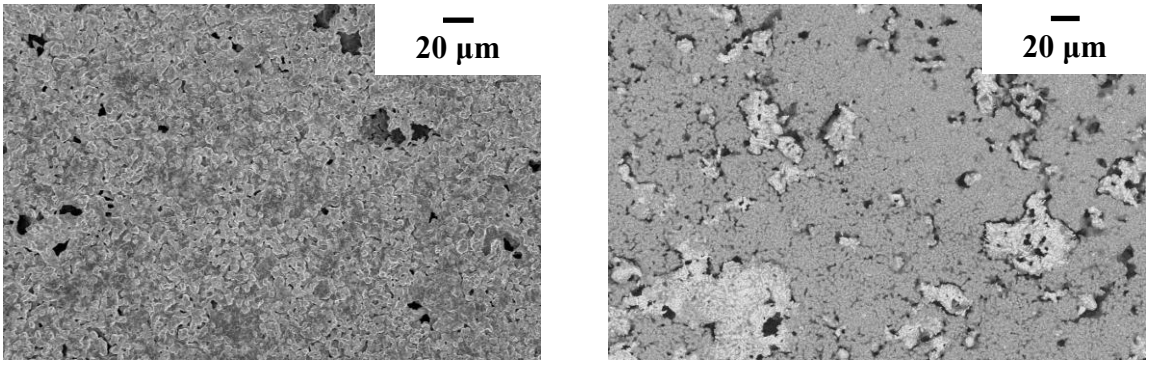

(a) (b)

Figure 9. Top view of sintered objects using SEM: (a) Secondary electron image (b) Backscattered electron image (note: places having high Ta concentration are shown as white spots). Powder mixture is 35wt% Ta + 65wt% ZrB_2. Laser parameters include 2 mm spot size, 150 W power and 0.6 mm/s scanning speed.

4. Si-ZrB_2 composite

Sintered ZrB_2-Si composite shows another type of surface morphology (Figure 10). We need to take a note that since Si is a brittle material, excessive stress can cause cracks (Figure 10(b)). Unlike ZrB_2-metal composites, where ductile metal portions are less susceptible to fracture, ZrB_2-Si samples may eventually break if the stress is not relieved. Accordingly, several samples have been broken either during sintering process or at microhardness test. Therefore, ZrB_2-metal composites are preferable because of their higher thermal shock resistance and fracture toughness.

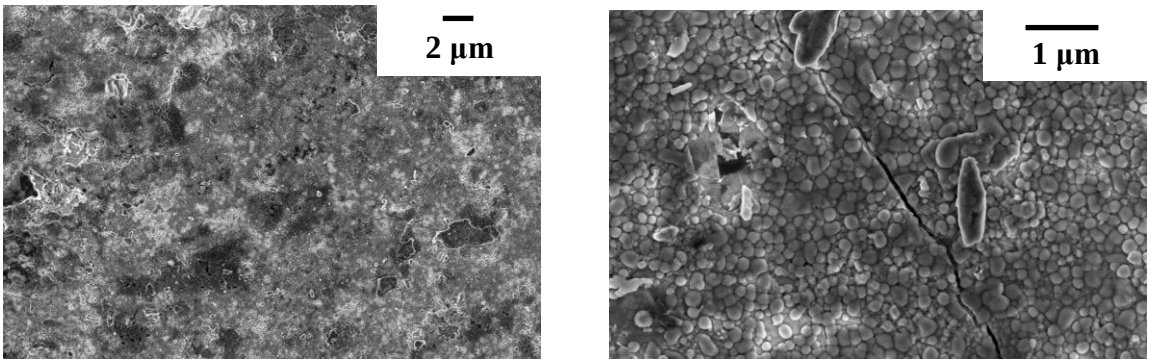

(a) (b)

Figure 10. SEM images (top view) of sintered objects (a) low magnification (b) close-up of the crack. Powder mixture is 50wt% Si + 50wt% ZrB_2.

vi. Chemical composition:

X-ray diffraction (XRD) technique is used to analyze crystal structures and chemical compositions of sintered samples. When using Zr and Si as binder materials, ZrB_2 and binders remain unchanged as separate phases and there is no new boride formation (Figure 11 and 14). But in the case of Ti and Ta binders, several borides are formed as shown in Figure 12 and 13. Nonetheless, some oxides formed because of the residual oxygen in the chamber. In addition, these commercially available powder materials have intrinsic thin surface oxide films as well.

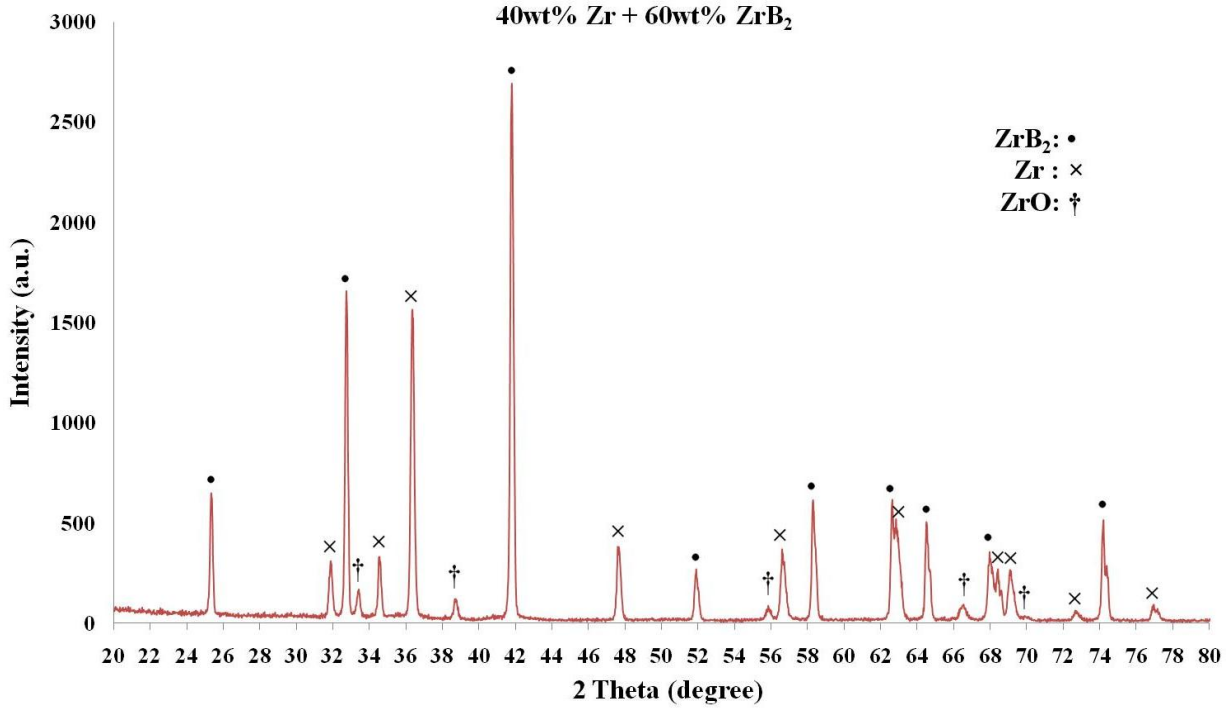

Figure 11. XRD result of 40wt% Zr + 60wt% ZrB_2.

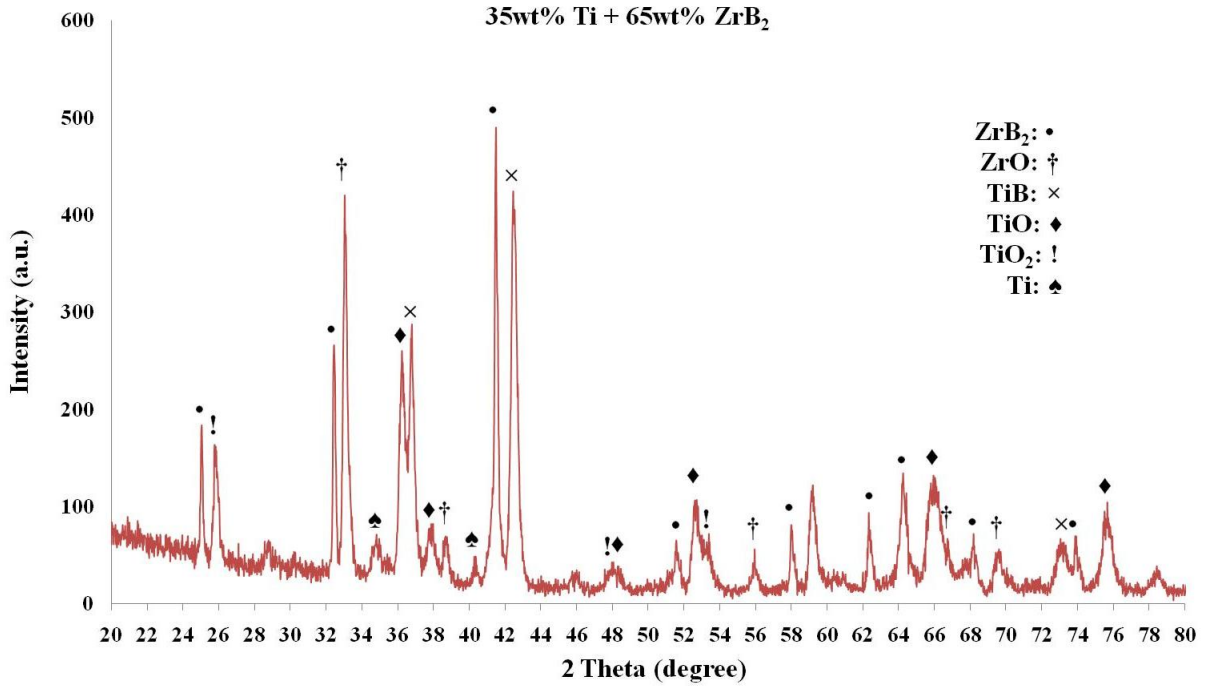

Figure 12. XRD result of 35wt% Ti + 65wt% ZrB_2.

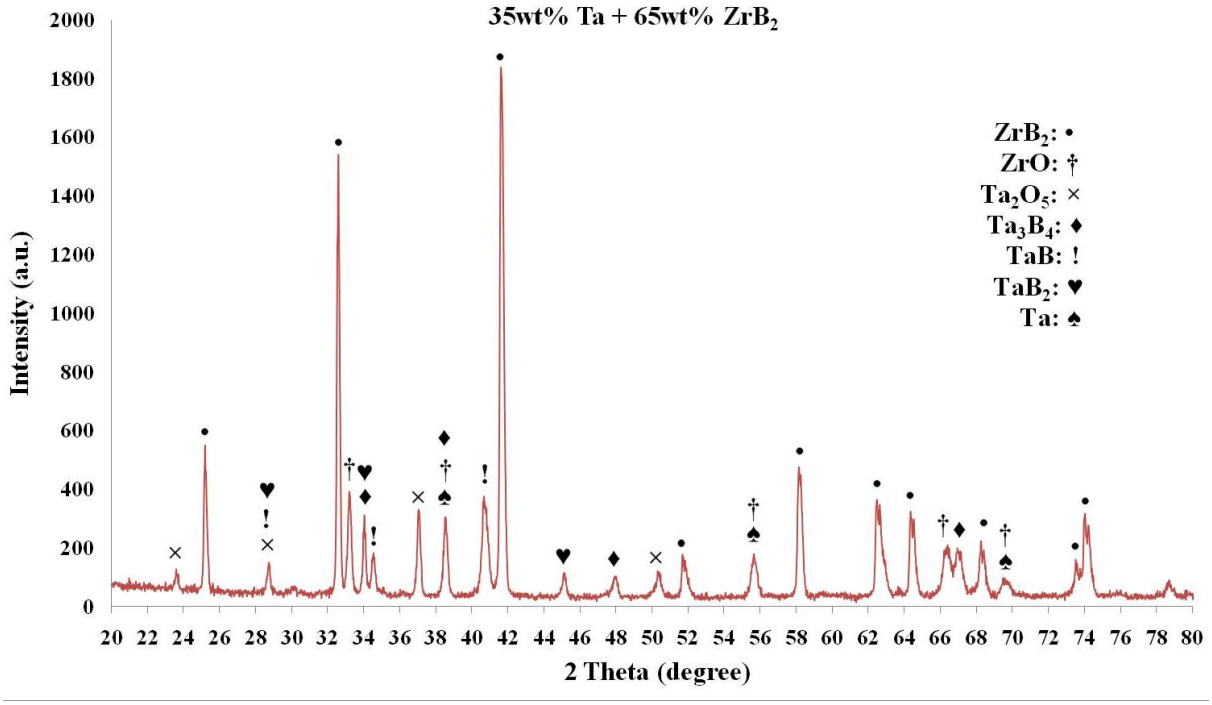

Figure 13. XRD result of 35wt% Ta + 65wt% ZrB_2.

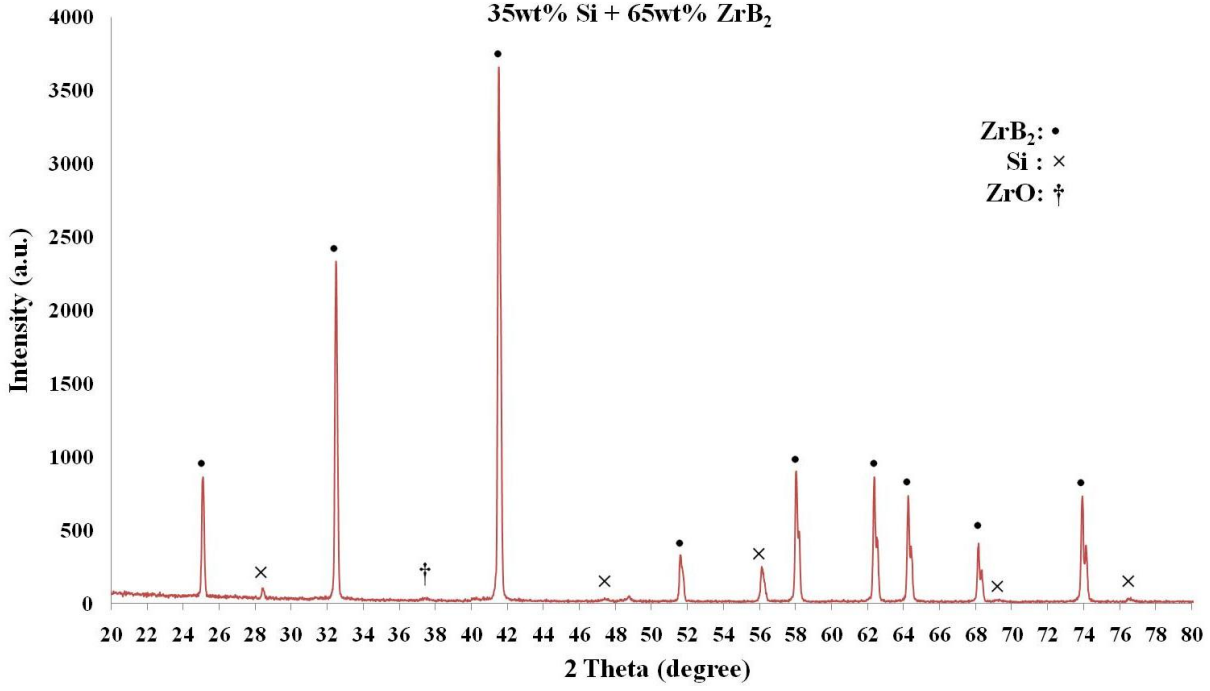

Figure 14. XRD result of 35wt% Si + 65wt% ZrB_2.

vii. Vickers microhardness test:

The hardness of ZrB_2-Zr composites measured near the ~22 GPa reported for pure ZrB_2 [4], despite Zr having a much lower hardness of ~1GPa [5]. ZrB_2-Si and ZrB_2-Ti composites possess similar hardness values, but arise from different reasons. Si is a hard material (~10GPa [6]), and since ZrB_2-Si doesn't form new phases as evidenced by its XRD result, the hardness value of ZrB_2-Si is expected to be between that of the individual components by the law of mixtures. However, ZrB_2 reacts with Ti during laser processing and forms TiB, itself a hard ceramic, so the hardness value of ZrB_2-Ti composite may in fact increase. For ZrB_2-Ta composite, although some new boride phases formed, the amount is relatively negligible because intensities in the XRD result seem to be very low. Therefore, its hardness will be lower since Ta is a relatively ductile metal. Lots of voids in ZrB_2-Ta sintered objects may also have a significant effect.

Table 3. Vickers microhardness test results (in GPa)

ZrB_2 (wt %)	Zr	Ta	Ti	Si
70 %	18.7	3.2	16.8	13.3
65 %	17.3	8.3	9	10
60 %	19			
50 %		7.6	11.3	11.8

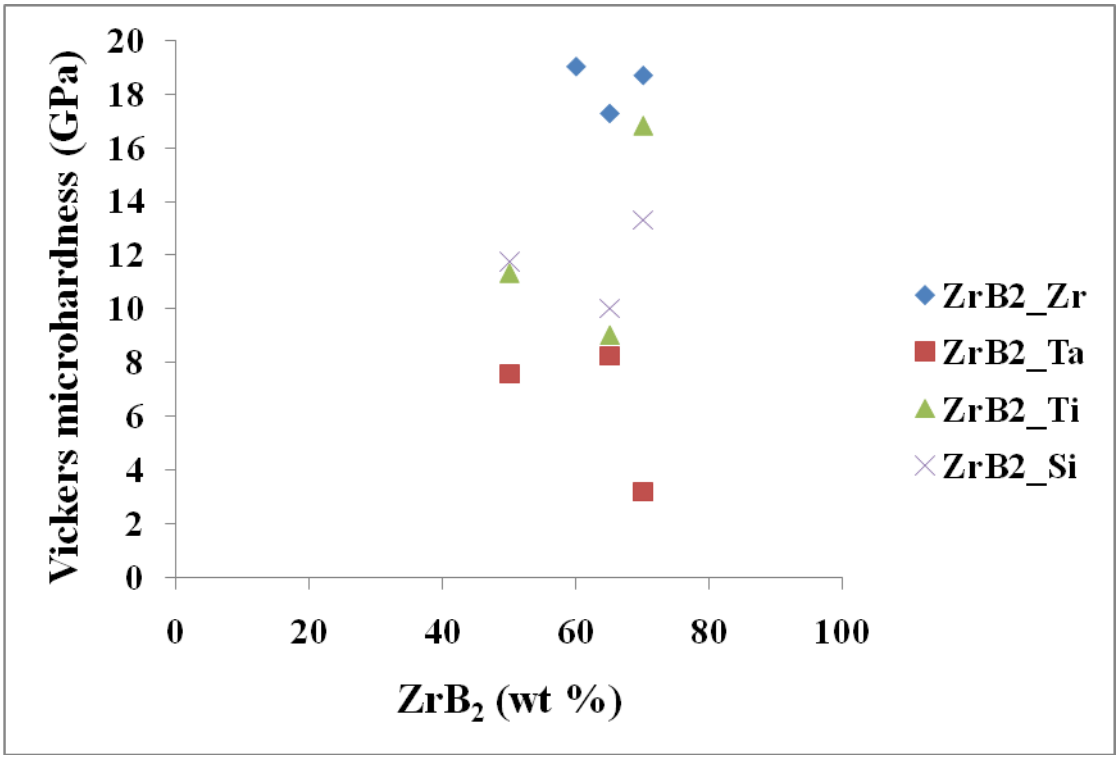

Figure 15. Vickers microhardness test results.

B. Microwave hybrid processing

i. Microwave heating:

1. Volumetric

Microwave absorption is proportional to the loss tangent of the radiated material. The loss tangent involves the material dielectric properties, and thus is frequency and temperature dependent. Polar molecules like water respond to the alternating electric field by undergoing rotation, which in turn causes heat. Metals can be directly heated due to electron response to the electromagnetic radiation, which results in resistive heating, however since the typical skin depth is very thin (<10μm) at 2.4GHz for high-conductivity materials, metals don't truly heat in a volumetric manner in a microwave. On the other hand, silicon carbide is a typical ceramic susceptor which improves microwave absorption of UHTCs at room temperature. In our studies, SiC was only used as an additive within the sample, not to re-radiate shorter wavelength energy (ie, ~1μm). Using 18 wt% SiC shortened the time necessary to process the sample when using the microwave + laser method, as ZrB_2 does not absorb microwaves efficiently at room temperature. Figure 16 shows a ZrB_2 sample in an alumina crucible that was heated via microwave radiation in an uncontrolled atmosphere. The ZrB_2 surface readily oxidizes to form B_2O_3, which has a high vapor pressure and thus provides little protection from further oxidation for temperatures above ~ 1200 °C [7]. As the boron outgases, the remaining zirconium reacts with oxygen to form ZrO_2. Zirconia absorbs microwaves more efficiently than ZrB_2 causing the entire sample to heat more rapidly, accelerating the rate of densification but with significant porosity and cracking of the ZrO_2 due to the B_2O_3 outgasing and zirconia's phase transformation upon cooling from very high temperatures, respectively.

Figure 16. ZrB_2 heated in air oxidizes to form ZrO_2.

2. Internal arcing

Despite being considered a ceramic, ZrB_2 has excellent electrical conductivity, comparable to iron or lead [8]. Therefore, applying an external electric field such as is done inside a microwave causes electrons to move across the sample in response to the electric field gradient. Due to the mode stirrers in the microwaves used in these experiments, the electric field

gradients at a given location cycle with time with a period of about 3 seconds. Maximum field potential occurs over a distance of ¼ wavelength, ~ 3 cm. When using samples a couple centimeters in diameter, strong arcing may result from the electrons moving between particles in the ZrB_2 powder. The powder size and packing density affect the total path resistivity, as an increase in the number of boundary layers between particles requires a higher applied field to achieve the same response. The powder particles have an inherent thin oxidation layer that insulates electron jumping until the applied field exceeds some critical threshold. Furthermore, the particle shape also impacts the probability of arcing. Our experiments used powder with ~15 μm and ~2 μm particle sizes, with both shaped very irregularly and with jagged edges. Therefore, the likelihood of arcing can be attributed to various conditions: a) the sharp points on the powder particles intensify the local field, b) the irregular particles are packed densely enough or are large enough to maintain a reasonable contact resistance, and c) the surface oxides on the powder are thick enough to prevent simple electron redistribution, but still thin enough to allow tunneling via arcing.

The volatile nature of arcing did not result in good densification of samples without additional heat sources, but it did provide an atmosphere for creating unique nanostructures. The intense arcing rapidly heats the sample, where the high field gradient promotes structures to self-assemble on the surface and/or substrate. Some structures appear to precipitate from a vapor-phase deposition, typically when alumina is in contact with the conductive powder.

Figure 17. Two metal plates used to promote arcing through a powder placed within the gap.

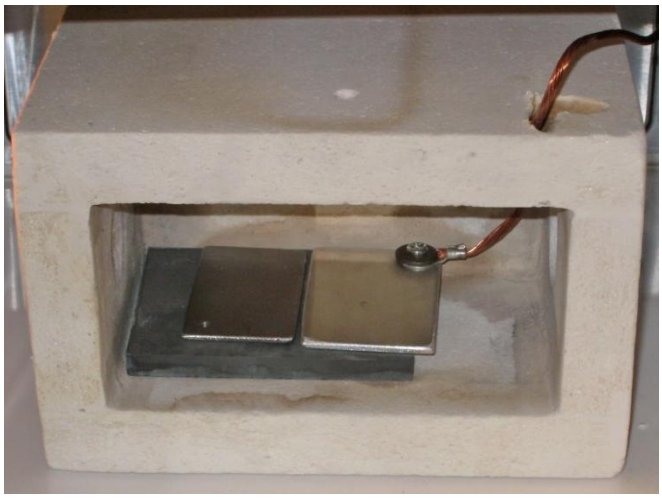

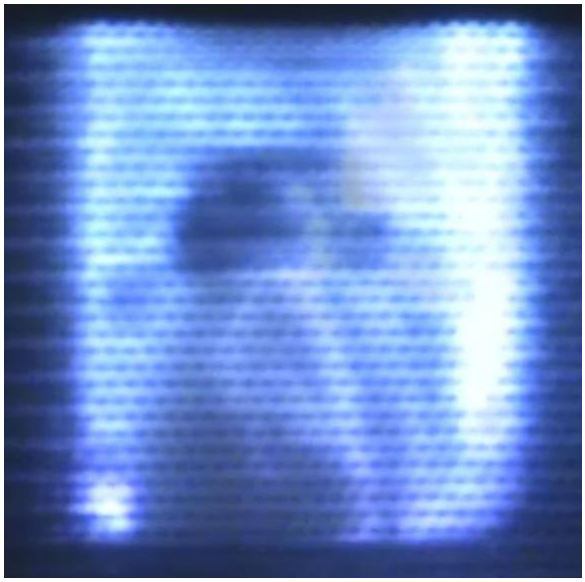

Figure 18. Arcing generates intense blue & white light emission within Muffle 2 after argon ionizes.

3. Enveloping arcing

Although not fully explored, arcing was also observed to occur within the entire volume of the ceramic muffle (#2). In this case, the arcing does not readily occur in air, instead initiating when argon is flowed into the muffle. The breakdown voltage of air is ~ 32 kV/cm, whereas argon is much lower at 2.7 kV/cm [9]. This method increases the temperature of the muffle to >500 °C, thus indirectly heating the sample. In combination with the laser heating and the increased microwave absorption at higher temperatures, good densification is possible for a thickness up to ~ 1 mm.

ii. Nanostructure formation:

The nanostructures formed were dependent upon the applied field of the microwave, however in some cases laser (hybrid) heating was applied and the associated heat may have intensified the growth. Conversely, when nanostructures were created with both laser and microwave, the direct laser irradiation typically appeared to disintegrate the structures more than stimulate growth. Figure 19 shows SEM images of ~15 μm ZrB_2 powder heated solely by microwave inside an alumina crucible. The powder was processed in air, and the structures were formed with only a few seconds of cumulative arcing time. Fig. 19(a) shows nanorod growth, likely an oxide as the SEM image exhibits surface charging. Also visible is a fiber mesh supporting the nanorods, which from multiple EDS results appears to be composed of boria. Fig. 19(b-d) show rectangular nanotubes grown near the previously smooth Al_2O_3 substrate, in some cases growing directly from the substrate. TEM/EDS analysis of structures like those in Fig. 19(b) had a compositional mix of Zr, Al, O and perhaps B. These rectangular nanotubes resemble those discovered by Kong, Wang & Wu [10] where each tube consisted of a single-crystal of mullite (Al, Si and O). In our case, the element Zr may have functionally replaced the Si to create a crystal structure similar to mullite. Fig. 19(c) shows an intricate structure grown from a single seed point, where the formation of some tubes clearly shows a multi-wall structure. Moreover, the rectangular nanorods in Fig. 19(d) do not appear to be hollow and have grown in a curved manner coming to a central point.

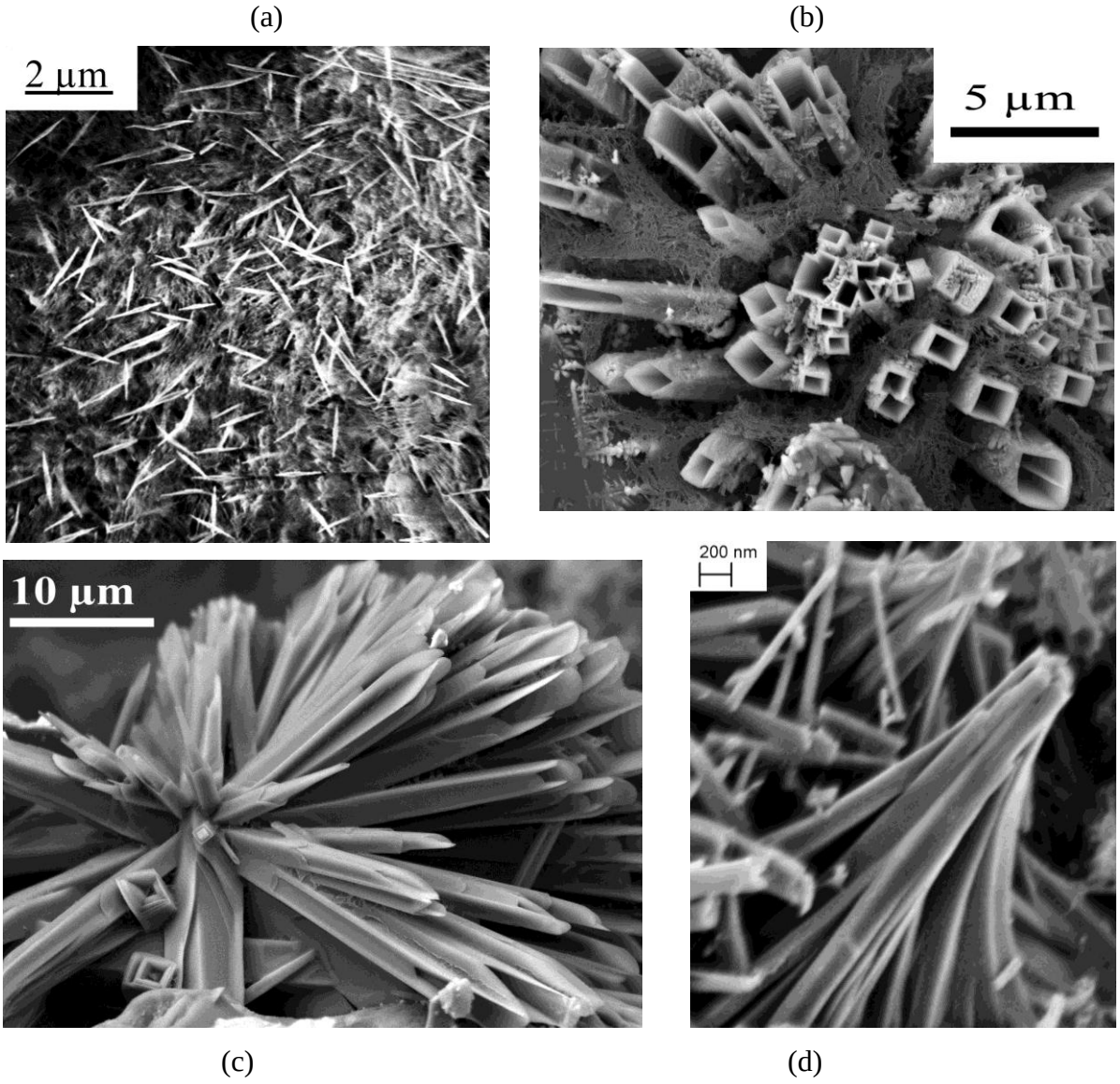

Figure 19. Nanostructure growth due to arcing of ZrB_2 powder in alumina crucible.

Figure 20 shows ZrB_2 powder hybrid processed with ~150W of laser power, with various compositions and substrates. Fig. 20(a) shows high aspect-ratio nanorods, many with a particle on the tip that may have facilitated growth. These nanorods grew directly from the mixture of ZrB_2 and 14 wt% Al_2O_3. Fig. 20(b) shows miniature versions of the rectangular nanotubes presented in Fig. 19(b), although again these tubes grew directly from the powder particles and not out of the substrate. This powder composition also included nickel, however the structure composition was not analyzed. In Fig. 20(c), a multitude of small crystal-like structures grew

from a ZrB_2 + SiC mixture on top of an alumina substrate. Fig. 20(d) shows the multi-directional growth of many rectangular nanorods, where the intersection of rods during formation didn't appear to alter their continued direction of growth. In both Fig. 20 (c) and (d) the growth seems dependent upon being in contact with the alumina substrate.

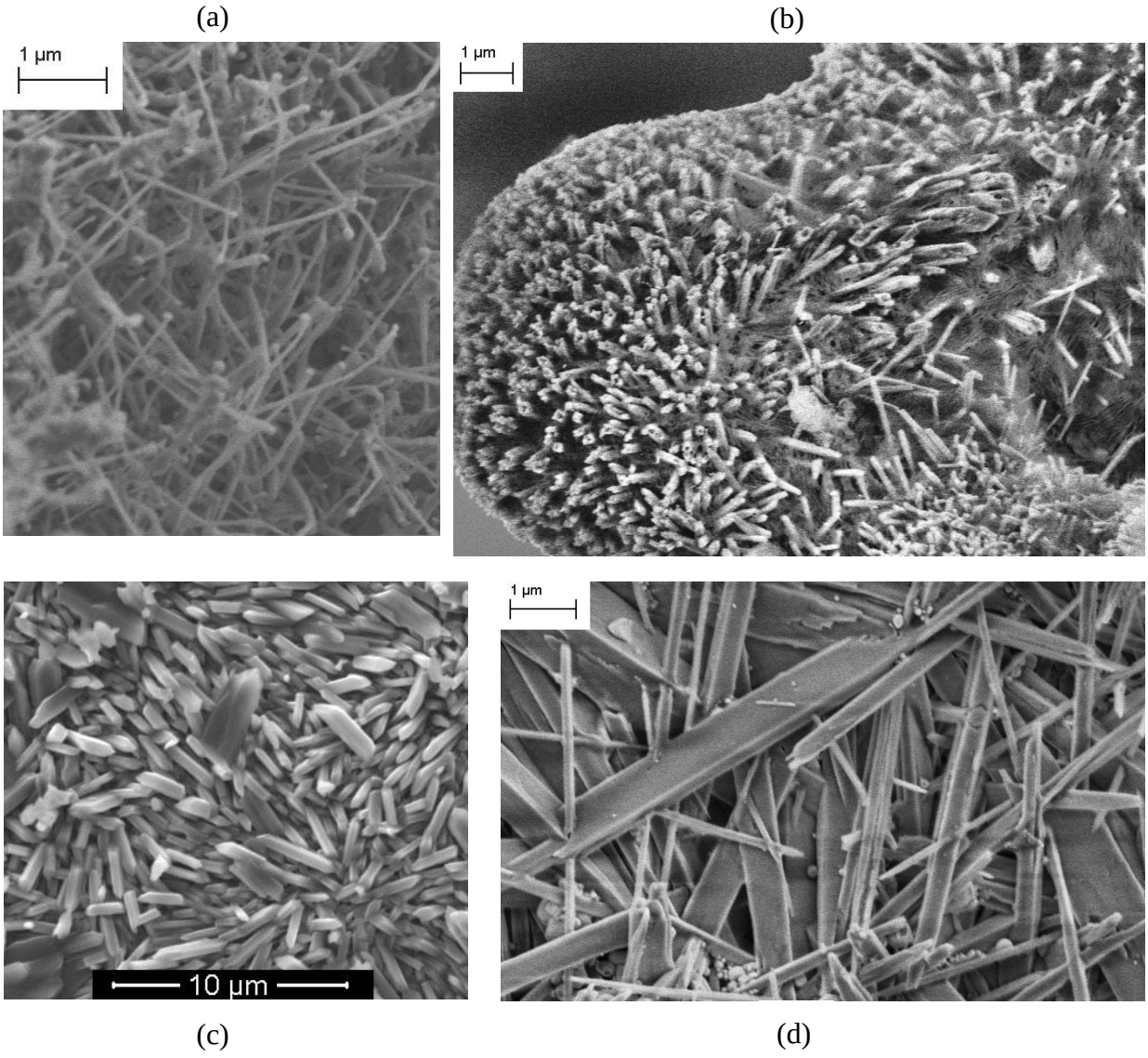

Figure 20. Nanostructures formed under hybrid processing using ZrB_2 powder with: (a) 14 wt% Al_2O_3 (b) 18 wt% Ni + 10 wt% Al_2O_3 (c) 18 wt% SiC (d) 20 wt% Ni. Fig. (a) & (b) are on Si_3N_4 substrate, whereas Fig. 20(c) & (d) are on alumina.

iii. Hybrid sintering

1. ZrB_2 in air

Heating ZrB_2 powder in air to temperatures significantly greater than 1000 °C results in the formation of zirconia on the sample surface. Typically the zirconia surface is porous due to the outgasing of B_2O_3. Moreover, the surface cracks due to significant volume shrinkage from the associated phase transformation during cooling. Fig. 21 (a) and (b) show zirconia surfaces formed when irradiated by ~100W of laser power and ~1050 W of microwave power for only 30 seconds. The laser spot size was ~3 mm in diameter. To both the naked eye and SEM, the surfaces appear to be glassy, as if the zirconia were in a viscous state. The viscous state implies that the zirconia reached its melting point of 2700 °C, a tremendous heating rate from room temperature in only 30 seconds.

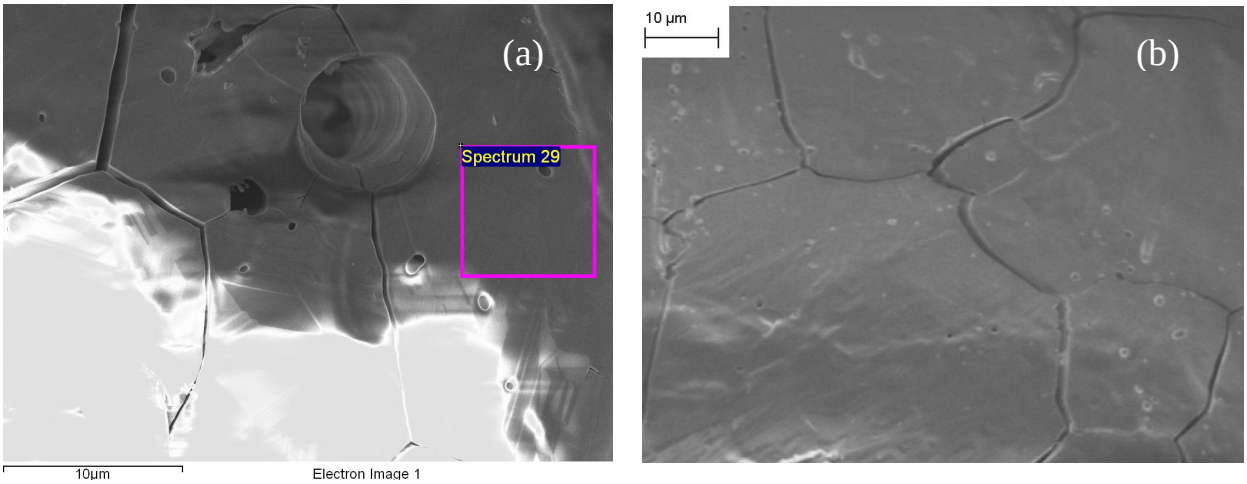

Figure 21. Samples of ZrB2 oxidized to zirconia and then sintered to a viscous state.

2. ZrB_2-SiC composite

Sintering ZrB_2 with 18 wt% SiC was possible in an argon environment. Arcing enveloped the sample, thus not all of the microwave power was available for volumetric heating of the SiC. After 180 seconds of heating with 166 W of laser power on a spot ~6 mm in diameter, the sample had begun densification, necking and grain growth. A longer processing time or higher density pressed starting powder may allow for full densification.

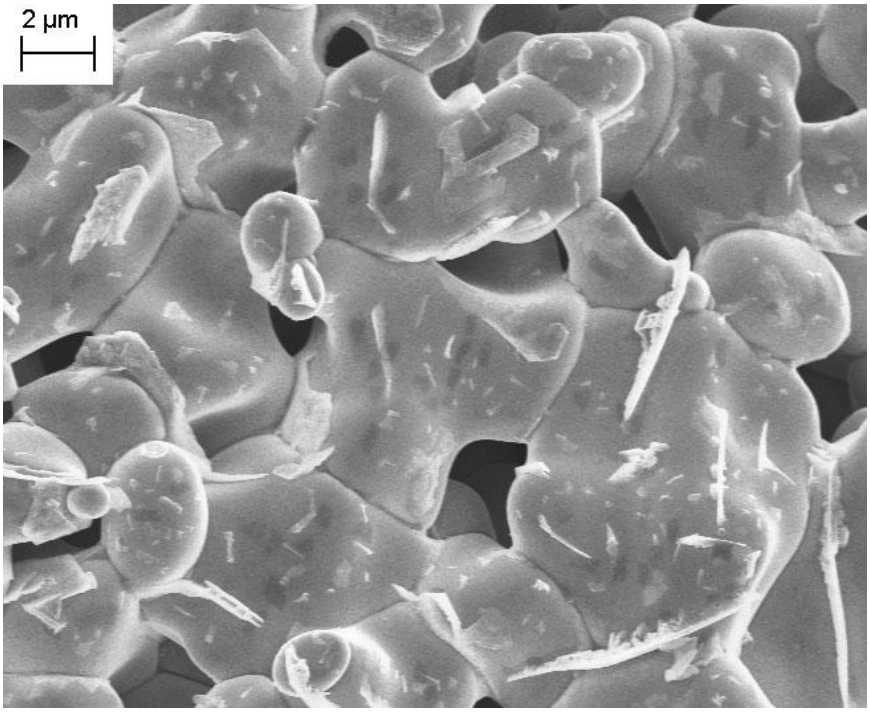

Figure 22. Partially sintered ZrB_2 + 18 wt% SiC after 180 seconds of hybrid processing.

3. ZrB_2-Zr composite

Excellent densification of the cermet ZrB_2 + 35 wt% Zr could be achieved in a matter of minutes using the hybrid heating method in argon. With a laser power of 166 W and a spot size of ~3.5 mm, Fig. 23 shows an SEM image of the sample surface after 120 seconds of processing. The same sample is shown as a visible picture in Fig. 24(b). The central area within the laser spot has good reflectivity, implying a relatively low surface roughness. The largest issue is the thermal stress involved with laser heating only a portion of the sample, discernible as the circular cracks just larger than the spot size. Fig. 24(a) shows a similar sample heated with a larger ~6 mm spot size but for 6 minutes of processing time instead of 2. The sample thickness was nearly 1.5 mm, however there was not sufficient power to get a strong bond throughout the entire thickness, and thus it was possible to crack the sample by hand.

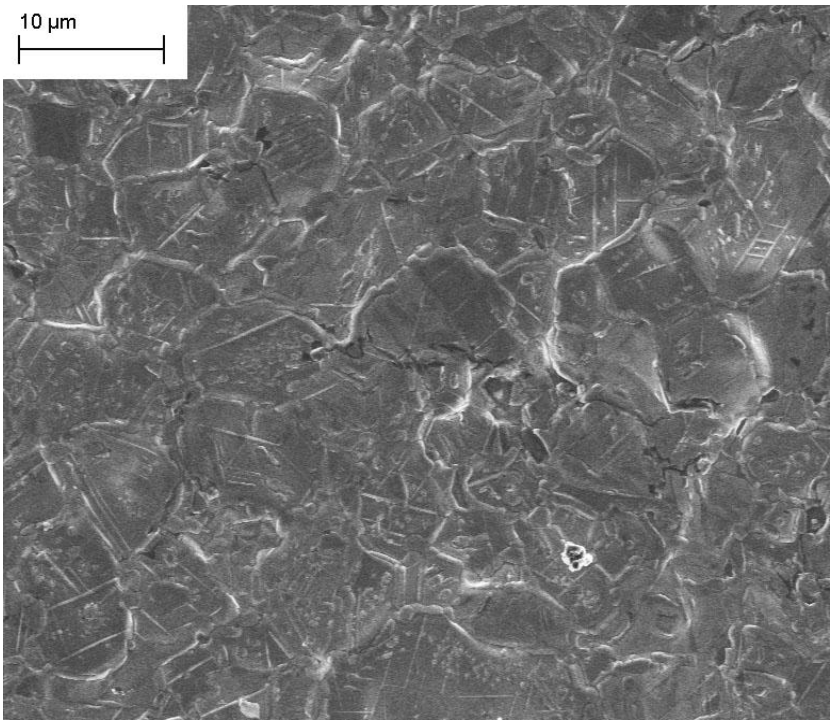

Figure 23. Sintered ZrB_2 + 35 wt% Zr after 120 seconds of heating.

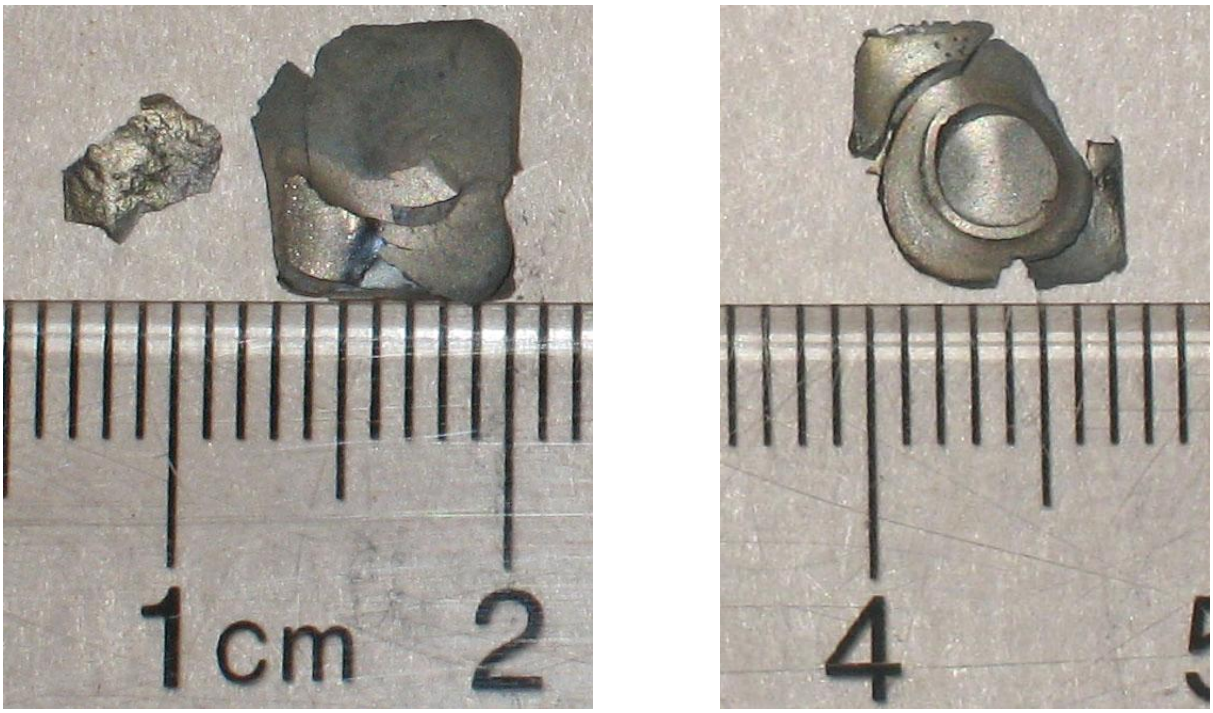

(a) (b)

Figure 24. Hybrid processed samples of ZrB_2 + 35 wt% Zr with 166 W of laser power for:
(a) 720 seconds with a spot size of ~ 6 mm (b) 120 seconds with a spot size of ~ 3.5mm.

iv. Chemical compositions

After the samples were processed, energy dispersive X-ray spectroscopy (EDS) was used to provide a qualitative analysis of elemental composition. EDS can provide a good estimate of relative contents of elements given a flat sample surface, appropriate excitation energy and an accurate standard for the composition being analyzed. In practice, our samples can range from reasonably flat to very rough, from high to low electrical conductivity for dissipating surface charges, and from perfectly to poorly matched standards. Rough samples will cause increased absorption of the x-ray signal by the sample itself. Low sample conductivity may prevent using a sufficient keV (excitation energy) to resolve heavier elements or may cause surface charging to reduce to the point where almost no resolution of features is possible. This is especially a problem in resolving ceramic oxide structures, but may be alleviated by applying a thin surface coating of carbon or else gold to help reduce charge buildup. Likewise, mixing heavy and light elements without a matching standard reduces the ability of the software to appropriately correct for relative sensitivities among elements, and is further complicated by having multiple elements present. Moreover, detecting light elements like boron with some quantitative accuracy requires high transmission through the detector window for the low-energy emission from light elements, a well-conditioned window that is free of ice build-up from being operated at liquid nitrogen temperatures , and even dispersion of the elements in the sample with respect to depth within the beam area. Even then, software correction factors must be applied to correct for non-linearity's as best as possible.

The Zeiss SEM used for analysis contains an Oxford Inca X-sight EDS detector with a Moxtek AP3.3 window material. The window is well suited to resolve light elements, thus this system is able to resolve boron although with limited sensitivity for boron and carbon. The window transmission curve for 0-1 keV is given in Fig. 25. Minimum beam diameter is 1-2 μm.

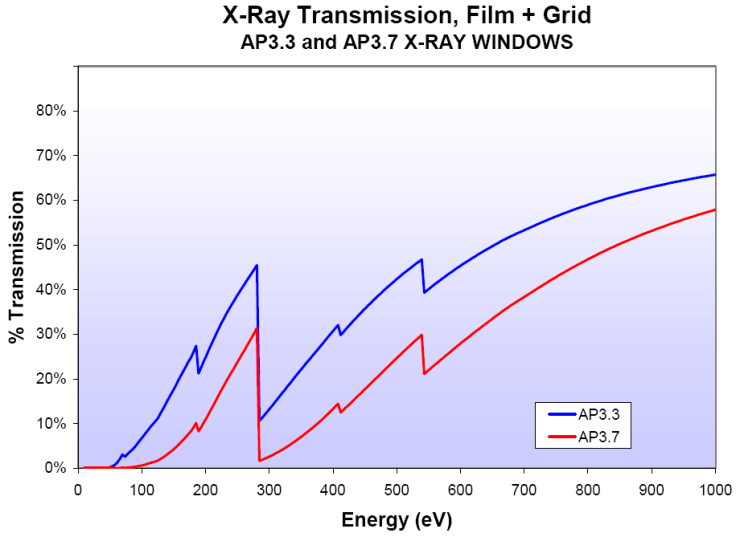

Figure 25. The blue (top) line indicates the transmission of our EDS detector window.
www.moxtek.com

To test the accuracy of reported ZrB_2 atomic composition, we analyzed a hot-pressed ZrB_2 sample supplied by Ceradyne. Fig. 26(a) shows an SEM image of the surface; the dark region is a boron-enriching particle. The uncorrected EDS count detection is shown in Fig. 26(b), and the final composition is given in Fig. 26(c). The atomic composition results typically ranged from 1:2 to 1:4 for Zr:B when forcing the software to normalize results for only those two elements. Adding C, N or O significantly lowered the accuracy and reliability of reported composition. Therefore, although EDS is extremely useful for understanding the sample composition, it cannot be expected to report accurate atomic composition for non-ideal specimens.

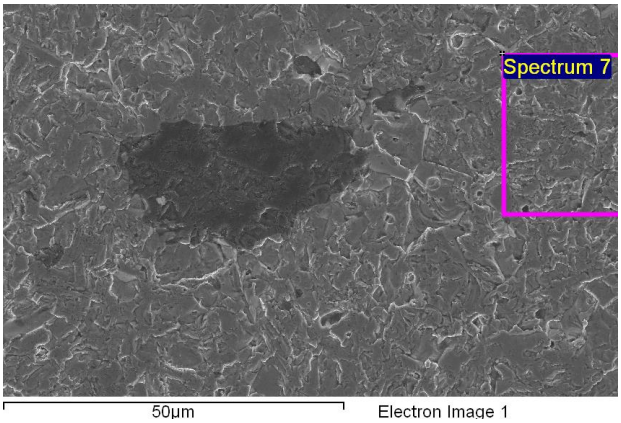

(a)

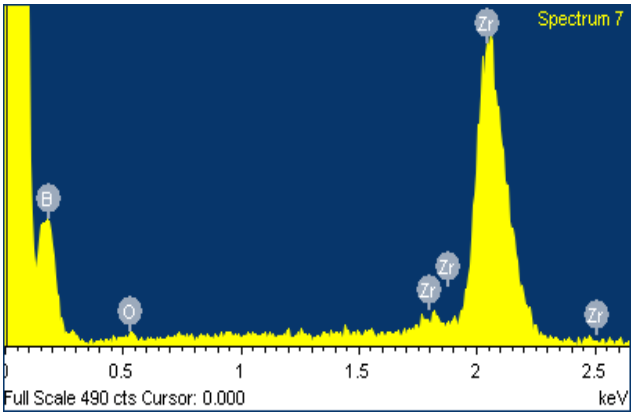

(b)

(c)

Element	Weight%	Atomic%
B K	22.5	69.0
O K	1.7	3.4
Zr L	75.9	27.6

Figure 26. Analysis of boron-enriched ZrB_2 sample supplied by Ceradyne: (a) SEM image (b) EDS counts (c) EDS composition

EDS results can help determine what interactions are occurring during processing. Fig. 27(a) shows a micron-sized ball formed when heating ZrB_2 + 18 wt% Ni on a stainless steel substrate. Arcing occurred between the powder and the substrate, forming the highly textured ball as well as a few smoother nanoballs on the surface of the larger ball. EDS analysis shows that the ball's surface is mostly boron oxide, a typical result when heating in air. The iron and chromium resulted from the arcing with the stainless, creating the smoother nanoballs. Fig. 27(b) shows the composition of the area of the magenta box labeled 'Spectrum 24.'

(a)

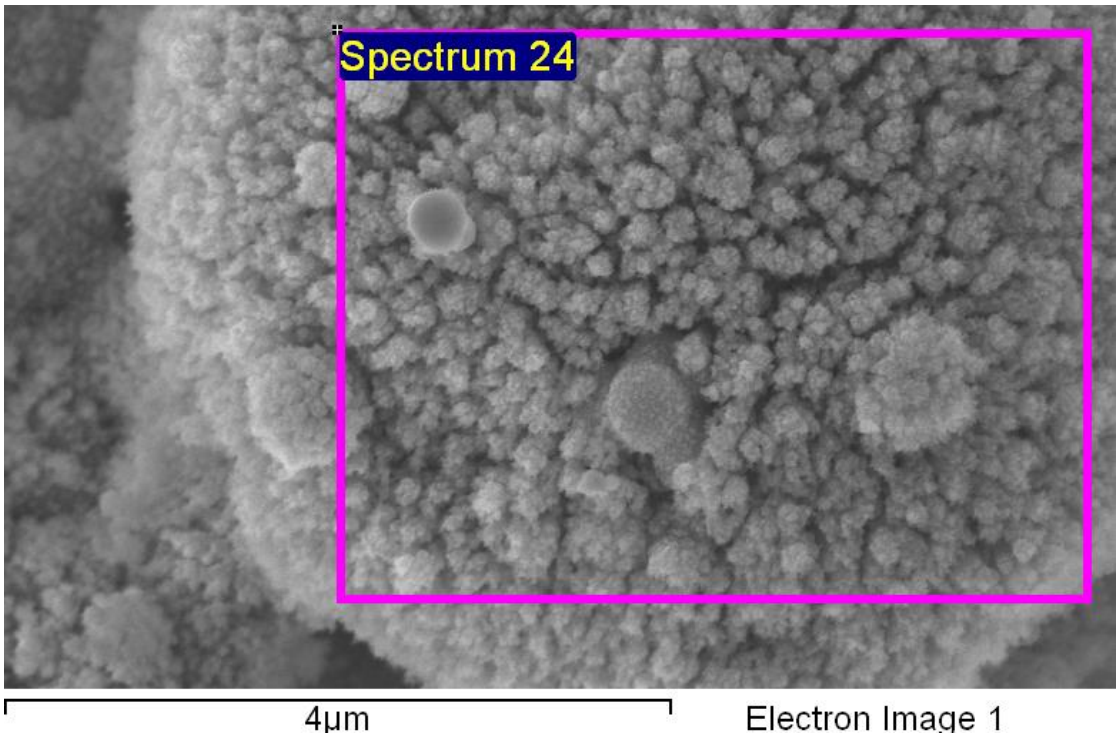

(b)

Element	Weight%	Atomic%
B K	12.3	27.0
C K	2.2	4.4
N K	1.1	1.9
O K	27.0	40.0
Al K	7.1	6.3
Cr L	7.2	3.3
Fe L	36.4	15.5
Zr L	6.6	1.7

Figure 27. ZrB_2 + 18 wt% Ni on stainless steel substrate, microwave processed for 20s: (a) SEM image of textured ball created during arcing (b) EDS composition.

While using the SEM, determining the homogeneity of the composition can be a useful tool. In Fig. 28(a) the SEM was used in backscatter imaging mode, which clearly differentiates between two particle types. This is in stark contrast to Fig. 22, which was taken on the same sample but in secondary electron mode. EDS was then employed to understand the segregation of materials. Fig. 28(b) shows that the lighter region in the SEM image can be approximated as zirconium diboride, whereas Fig. 28(c) shows the darker region to be approximately B_4C. These results would not have been obvious otherwise, as the starting powders were ZrB_2 and SiC. In

hybrid sintering the two powders in argon for 3 minutes, the SiC dissociated, with the carbon reacting with either boron oxide or zirconium diboride to form a boron carbide.

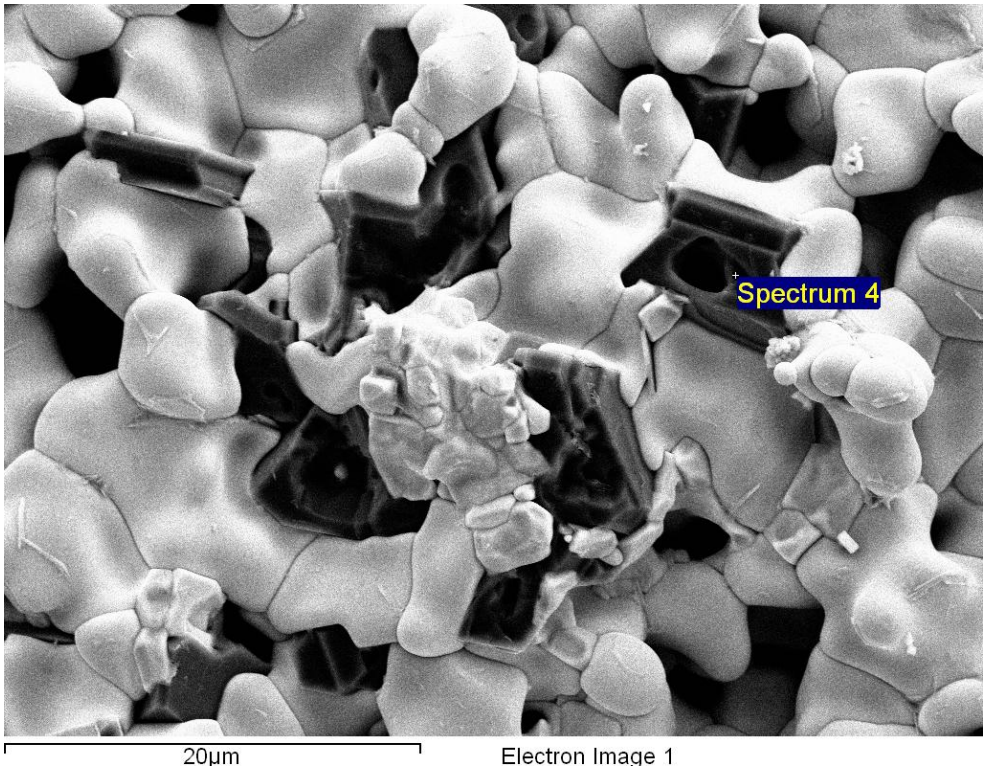

(a)

Light Region

Element	Weight%	Atomic%
B K	22.6	66.8
C K	2.7	7.1
Zr L	74.8	26.2

(b)

Dark Region

Element	Weight%	Atomic%
B K	74.3	76.7
C K	24.7	23.0
Si K	1.0	0.4

(c)

Figure 28. Hybrid sintering of ZrB_2+18 wt% SiC: (a) SEM backscatter image showing ZrB_2 grain growth in the lighter regions and interspersed B_4C formations in the dark regions (b) EDS results of light region (c) EDS results of dark region.

III. CONCLUSIONS

- Laser sintering experimental setup was completed.
- Microwave sintering experimental setup was completed.
- Laser + microwave (hybrid) sintering experimental setup was completed.
- Results on laser sintering of ZrB_2 powder were obtained and published in *Journal of American Ceramic Society* (C.N. Sun, M.C. Gupta, "Laser Sintering of ZrB_2," *Journal of the American Ceramic Society*, v 91, n 5, pp.1729-1731, 2008). High thermal stress generated during laser sintering, thus limited the applicability for large area. This problem was resolved by pre-heating the sample using induction heating technique and mixing with metals (Zr or Ti) to enhance the thermal shock resistance and fracture toughness.
- ZrB_2-metal composites have been successfully fabricated through laser sintering technique although minor voids exist within sintered objects; the density is still greater than 98% of theoretical values. ZrB_2-Zr has Vickers microhardness values closely follow the rule of mixtures, which fall in between hard ZrB_2 and soft Zr. Other ZrB_2 cermet composites have lower hardness values. XRD results show that new phases like metal borides are formed in ZrB_2-Ti and ZrB_2-Ta mixtures. In comparison, ZrB_2-Zr mostly retains its crystalline phases in the sintered sample. Moreover, some oxides have been formed because residual oxygen inside the chamber reacted with ZrB_2-metal composites. A manuscript discussing results on ZrB_2-Zr composite has been submitted to *Materials Letters* for publication. Second manuscript regarding ZrB_2-Ti composite is prepared for publication in *Journal of Materials Science* (attached with this report).
- Results on laser + microwave (hybrid) sintering were obtained and novel nanostructures were observed and were published in *Nanotechnology* (Tyson Baldridge, M.C. Gupta, "Zirconium Diboride Nanofiber Generation Via Microwave Arc Heating," *Nanotechnology*, v 19, n 27, 2008). A second manuscript is attached ("Nanostructure Formation from Zirconium Diboride & Alumina Precursors via Microwave Arc Heating" to be submitted to *Small*).
- Electron beam sintering of ZrB_2 was successfully carried out and results are described in attached manuscript (C. Sun, M.C. Gupta, K. Taminger, "Electron beam sintering of Zirconium diboride", to be submitted to *Materials Letters*).
- The laser and electron beam seem to be capable of melting ZrB_2 powder and even creating melt pools. Crystalline phases were mostly retained in the sintered layer, although oxidation, decomposition and selective volatilization may have slightly affected the formation of ZrO_x in laser system and elemental Zr in e-beam sintering system. Microwave processing needs auxiliary energy input to stimulate absorption. Arcing within the powder creates some

densification, but also generates nanostructures and significant variation in surface morphology

- Spiral laser scanning patterns have been adopted to minimize structural deformation. To further decrease thermal stress and improve sintering/melting performance, the electromagnetic induction method has been employed to provide additional heating. Alternatively, laser plus microwave hybrid heating can also provide a means to achieve good densification of ceramic metal composites with reduced residual stress.

In summary, with the help of binder materials and auxiliary heat inputs, we are able to produce highly-densified ZrB_2-metal composites using laser processing technique. Our next goals are testing oxidation resistance and modifying ZrB_2-metal composites through the addition of SiC, WC, etc. Functional gradings, alternating-layer structures and coatings are also under consideration for future work.

IV. REFERENCES

[1] W. G. Fahrenholtz, G. E. Hilmas, I. G. Talmy, et. al., "Refractory Diborides of Zirconium and Hafnium," *J. Am. Ceram. Soc.*, v 90, n 5, pp 1347-1364, 2007, DOI 10.1111/j.1551-2916.2007.01583.x.

[2] D. Sciti, F. Monteverde, S. Guicciardi, et. al., "Microstructure and Mechanical Properties of ZrB2–MoSi2 Ceramic Composites Produced by Different Sintering Techniques," *Mater. Sci. Eng. A*, v 434, n [1–2], pp 303–309, 2006, DOI 10.1016/j.msea.2006.06.112.

[3] A. Bellosi, F. Monteverde, "Fabrication and Properties of Zirconium Diboride-based Ceramics for UHT Applications," *Hot Structures and Thermal Protection Systems for Space Vehicles, Proceedings of the 4th European Workshop held 26-29 November, 2002 in Palermo, Italy*, 2003, p 65. [link]

[4] J.V. Rau, D. Ferro, M.B Falcone, et al., "Hardness of zirconium diboride films deposited on titanium substrates," *Materials Chemistry and Physics*, v 112, n 2, pp 504-509, 2008. DOI 10.1016/j.matchemphys.2008.06.004

[5] E.M. Savitsky, Oleg D. Sherby, The Influence of Temperature on the Mechanical Properties of Metals and Alloys, Stanford University Press, p 151, 1961.

[6] Robert Hull, Properties of Crystalline Silicon, EMIS Datareview n 20, Institution of Engineering and Technology, p 137, 1999.

[7] Fei Peng, Robert Speyer, "Oxidation Resistance of Fully Dense ZrB_2 with SiC, TaB_2, and $TaSi_2$ Additives," *J. Am. Ceram. Soc.*, v 91, n 5, pp 1489–1494, 2008, DOI 10.1111/j.1551-2916.2008.02368.x.

[8] Tyson Baldridge, M.C. Gupta, "Zirconium Diboride Nanofiber Generation Via Microwave Arc Heating," *Nanotechnology*, v 19, n 27, 2008, DOI 10.1088/0957-4484/19/27/275601.

[9] Guo Li, He-Ping Li, Wen-Ting Sun, et. al., "Discharge features of radio-frequency, atmospheric-pressure cold plasmas under an intensified local electric field," *J. Phys. D: Appl. Phys.*, v 41, n 20, p 202001, 2008, DOI 10.1088/0022-3727/41/20/202001.

[10] X.Y. Kong, Z.L. Wang, Jiansheng Wu, "Rectangular Single-Crystal Mullite Microtubes" *Adv. Mater.*, v 15, n 17, pp 1445-1449, 2003, DOI 10.1002/adma.200305405.

V. Publications Generated During This Program:

[1] C.N. Sun, M.C. Gupta, "Laser Sintering of ZrB_2," *Journal of the American Ceramic Society*, v 91, n 5, pp.1729-1731, 2008, DOI 10.1111/j.1551-2916.2008.02369.x

[2] Tyson Baldridge, M.C. Gupta, "Zirconium Diboride Nanofiber Generation Via Microwave Arc Heating," *Nanotechnology*, v 19, n 27, 2008, DOI 10.1088/0957-4484/19/27/275601

[3] C.N. Sun, M.C. Gupta, "Laser Sintering of Ultra High Temperature Ceramics (ZrB_2)," *9th International Symposium on Laser Precision Microfabrication*, Québec, Canada, June 16-20, 2008.

[4] Tyson Baldridge, M.C. Gupta, "Laser + Microwave Hybrid Processing of Ceramic Materials," *9th International Symposium on Laser Precision Microfabrication*, Québec, Canada, June 16-20, 2008.

[5] C.N. Sun, T. Baldridge, M.C. Gupta, "Microstructures and Mechanical Properties of ZrB2-Zr Composite Formed by Laser Sintering / Melting Technique" (under review by Materials Letters).

[6] C.N. Sun, T. Baldridge, M.C. Gupta, " Laser Sintering / Melting of TiB Fiber-Reinforced ZrB2-Ti Composite" (under preparation for Journal of Materials Science).

[7] C.N. Sun, M.C. Gupta, K. Taminger, "Electron Beam Sintering of Zirconium Diboride" (under preparation).

[8] Tyson Baldridge, C.N. Sun, M.C. Gupta, "Nanostructure Formation from Zirconium Diboride & Alumina Precursors via Microwave Arc Heating," (under preparation).